Muon creation in supernova matter facilitates neutrino-driven explosions

R. Bollig,[1,2] H.-T. Janka,[1] A. Lohs,[3] G. Martínez-Pinedo,[3,4] C.J. Horowitz,[5] and T. Melson[1]

[1] *Max-Planck-Institut für Astrophysik, Karl-Schwarzschild-Str. 1, 85748 Garching, Germany*
[2] *Physik Department, Technische Universität München, James-Franck-Str. 1, 85748 Garching, Germany*
[3] *GSI Helmholtzzentrum für Schwerionenforschung, Planckstraße 1, 64291 Darmstadt, Germany*
[4] *Institut für Kernphysik (Theoriezentrum), Technische Universität Darmstadt, Schlossgartenstraße 2, 64289 Darmstadt, Germany*
[5] *Nuclear Theory Center and Department of Physics, Indiana University, Bloomington, IN 47408*

Muons can be created in nascent neutron stars (NSs) due to the high electron chemical potentials and the high temperatures. Because of their relatively lower abundance compared to electrons, their role has so far been ignored in numerical simulations of stellar core collapse and NS formation. However, the appearance of muons softens the NS equation of state, triggers faster NS contraction and thus leads to higher luminosities and mean energies of the emitted neutrinos. This strengthens the postshock heating by neutrinos and can facilitate explosions by the neutrino-driven mechanism.

arXiv:1706.04630v2 [astro-ph.HE] 17 Nov 2017

Introduction.—First state-of-the-art three-dimensional (3D) simulations have recently yielded successful supernova (SN) explosions by the neutrino-driven mechanism [1–8]. But the explosions turned out to be more delayed than in two-dimensional (axisymmetric; 2D) calculations and sensitive to neutrino effects even on the 10–20% level [3]. Accurate physics in the neutrino and nuclear sectors is therefore demanded to investigate the viability of the neutrino-driven mechanism by self-consistent, first-principle neutrino-hydrodynamical simulations.

While the presence of muons is well known to play a role in cold neutron stars (NSs; e.g. [9, 10]), it is traditionally ignored in SN matter based on the argument that the high muon rest mass ($m_\mu c^2 \approx 105.66\,\mathrm{MeV}$) suppresses their formation. This reasoning, however, is not well justified [11] because the electron chemical potential in newly formed NSs exceeds the muon rest mass, and the peak temperatures rise above 30 MeV after roughly 100 ms after core bounce, when the thermal distributions of photons and neutrinos reach well beyond 100 MeV. These conditions enable the production of significant numbers of muons and anti-muons (μ^-, μ^+) via electromagnetic interactions such as $e^- + e^+ \longrightarrow \mu^- + \mu^+$ and $\gamma + \gamma \longrightarrow \mu^- + \mu^+$ (γ denotes high-energy photons), via weak reactions that couple the e-lepton and μ-lepton sectors, and via β-processes between nucleons and muon neutrinos and antineutrinos (ν_μ, $\bar{\nu}_\mu$), which are created in the SN core through thermal pair processes.

While the new-born NS loses electron-lepton number by radiating a slight excess of electron neutrinos (ν_e) compared to electron anti-neutrinos ($\bar{\nu}_e$), it also gradually builds up net muon-lepton number ("muonizes") by emitting more muon antineutrinos than muon neutrinos. Electrons and muons thus share the negative charge that compensates the positive reservoir of protons (and of some e^+ and μ^+). Here we show that the rearrangements in the stellar medium and the neutrino emission that are associated with the appearance of muons have an important impact on the evolution of the proto-NS by accelerating its contraction. This facilitates the development of SN explosions by the neutrino-driven mechanism. Muons therefore must be included in self-consistent, first-principle models of the SN phenomenon.

Neutron star formation with muons.—Assuming neutrino-flavor oscillations do not play a role, conservation equations for the lepton numbers (i.e., the numbers of the charged leptons plus their neutrinos minus those of the corresponding anti-particles) for all three flavors hold individually. During stellar core collapse neutrinos get trapped and equilibrate at about one percent of the nuclear saturation density ($\rho_0 \approx 2.7 \times 10^{14}\,\mathrm{g\,cm^{-3}}$ or baryon density $n_0 \approx 0.16\,\mathrm{fm^{-3}}$). Subsequently, they diffuse out of the newly formed NS only over a time scale of several seconds. The NS, which begins to form at core bounce, thus inherits a large concentration of electron-lepton number from the progenitor core with an initial electron-flavor lepton fraction of ∼0.30 electrons plus electron neutrinos per baryon [12]. The diffusive loss of ν_e then drives the evolution to the final neutron-rich state of a cold NS with its small remaining content of protons.

In contrast, the trapped muon and tau-lepton numbers are zero initially. The τ density remains extremely small at all times because of the huge rest mass of the tauons ($m_\tau c^2 \approx 1777\,\mathrm{MeV}$), which is much bigger than both the temperature and electron chemical potential in the NS. Therefore the ν_τ and $\bar{\nu}_\tau$ numbers are initially equal and the chemical potentials $\mu_{\nu_\tau} = -\mu_{\bar{\nu}_\tau} = 0$ with high precision. However, since the cross section for neutral-current scattering with nucleons, $\nu + N \longrightarrow \nu + N$ ($N = n, p$), is somewhat larger for neutrinos than for anti-neutrinos due to weak-magnetism corrections (of order $\epsilon/(m_N c^2)$ with neutrino energy ϵ and nucleon mass m_N; [13]), $\bar{\nu}_\tau$ diffuse out faster and the proto-NS is expected to (transiently) develop a considerable tau-lepton number in the neutrino sector ($\mu_{\nu_\tau} > 0$) even though the formation of tauons is negligible [14].

Different from tau neutrinos, but analogously to ν_e and

TABLE I. Neutrino reactions with muons.

$\nu + \mu^- \rightleftarrows \nu' + \mu^{-\prime}$	$\nu + \mu^+ \rightleftarrows \nu' + \mu^{+\prime}$
$\nu_\mu + e^- \rightleftarrows \nu_e + \mu^-$	$\bar{\nu}_\mu + e^+ \rightleftarrows \bar{\nu}_e + \mu^+$
$\nu_\mu + \bar{\nu}_e + e^- \rightleftarrows \mu^-$	$\bar{\nu}_\mu + \nu_e + e^+ \rightleftarrows \mu^+$
$\bar{\nu}_e + e^- \rightleftarrows \bar{\nu}_\mu + \mu^-$	$\nu_e + e^+ \rightleftarrows \nu_\mu + \mu^+$
$\nu_\mu + n \rightleftarrows p + \mu^-$	$\bar{\nu}_\mu + p \rightleftarrows n + \mu^+$

$\bar{\nu}_e$, ν_μ and $\bar{\nu}_\mu$, participate in β-reactions,

$$\nu_\ell + n \rightleftarrows p + \ell^- , \quad (1)$$

$$\bar{\nu}_\ell + p \rightleftarrows n + \ell^+ , \quad (2)$$

with their charged leptons, ℓ (standing for e or μ), when a significant population of thermally excited μ^- and μ^+ appears [11]. Beta equilibrium for both flavors implies the usual relation

$$\Delta\mu \equiv \mu_n - \mu_p = \mu_\ell - \mu_{\nu_\ell} \quad (3)$$

between the chemical potentials (including particle rest-mass energies) of neutrons, protons, charged leptons, and the corresponding neutrinos. Since the highly degenerate Fermi sea of e^- partially converts to μ^-, and since initially the trapped muon number is zero, an excess of μ^- over μ^+ is compensated by an opposite excess of $\bar{\nu}_\mu$ over ν_μ. Therefore the diffusive flux of $\bar{\nu}_\mu$ will dominate that of ν_μ, leading to a gradual build-up of muon number. The easier escape of $\bar{\nu}_\mu$ compared to ν_μ is aided by the lower neutral-current scattering cross section for $\bar{\nu}_\mu$ mentioned above and by the higher opacity for β-reactions of ν_μ compared to $\bar{\nu}_\mu$ in analogy to the electron-flavor. The accumulation of net muon number in the proto-NS, i.e. the process of muonization that leads to an excess of μ^- over μ^+ in the final NS, is facilitated by the reactions of Eqs. (1) and (2). Also other interactions that couple the e-lepton and μ-lepton sectors (Table I) enhance the muonization rate and thus increase both the ν_μ and $\bar{\nu}_\mu$ fluxes.

Muonization might play a non-neglible role during all stages of the SN post-bounce (p.b.) evolution and NS as well as black-hole (BH) formation. In the following we discuss its effects on the initiation of SN explosions by neutrino-energy deposition.

Numerical modeling.—Our SN simulations were performed with the PROMETHEUS-VERTEX neutrino-hydrodynamics code [15, 16] with an approximate treatment of general relativistic gravity by the effective gravitational potential of Case A of [17]. The PROMETHEUS hydrodynamics module solves the equations of non-relativistic hydrodynamics (continuity equations for mass, momentum, energy, lepton number, and nuclear composition) with an explicit, directionally-split, higher-order Godunov scheme [18]. The transport module VERTEX integrates the energy-dependent evolution equations of energy and momentum for all six neutrino species (ν_e, $\bar{\nu}_e$, ν_μ, $\bar{\nu}_\mu$, ν_τ, $\bar{\nu}_\tau$) in the comoving frame of the stellar fluid to order v/c (v is the fluid velocity, c the speed of light), including corrections due to general relativistic redshift and time dilation. The closure is provided by an Eddington factor based on the solution of a model-Boltzmann equation, iterated for convergence with the set of two-moment equations [15]. Neutrino transport in multi-dimensional simulations employs the ray-by-ray plus approximation [16].

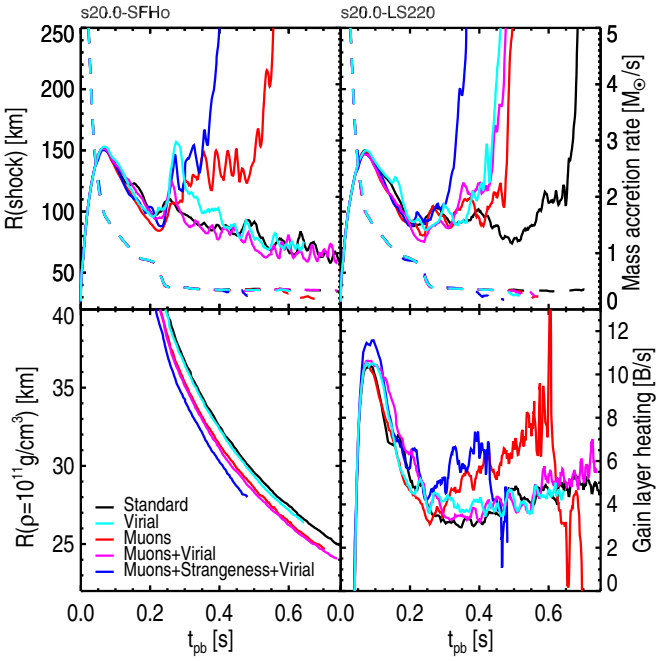


FIG. 1. *Upper row:* Angle-averaged shock radii (solid) and mass-infall rates (at 400 km; dashed) vs. post-bounce time for our sets of models with SFHo (*left*) and LS220 EoS (*right*). *Lower row:* Time evolution of NS radii (measured at an average density of $10^{11}\,\mathrm{g\,cm^{-3}}$; *left*) and net heating rate integrated over the gain layer (in $1\,\mathrm{B\,s^{-1}} = 10^{51}\,\mathrm{erg\,s^{-1}}$; *right*) for models with SFHo EoS.

We upgraded the PROMETHEUS-VERTEX code for including all effects of μ^- and μ^+ in the hydrodynamics and equation of state (EoS) of the stellar plasma, the effective relativistic gravity potential, and in the neutrino transport. This implies the solution of conservation equations for electron and muon lepton number:

$$\frac{\partial(\rho Y_\ell)}{\partial t} + \boldsymbol{\nabla}(\rho Y_\ell\, \boldsymbol{v}) = Q_\ell \quad (4)$$

(here relativistic corrections are omitted for simplicity). $Y_\ell = Y_{\ell^-} - Y_{\ell^+}$ is the net number of charged leptons per nucleon, ρ the baryon-mass density and Q_ℓ the source rate that is associated with all processes emitting and absorbing ν_ℓ and $\bar{\nu}_\ell$. The EoS depends on Y_e and Y_μ, i.e., $P = P(\rho, T, Y_e, Y_\mu, \{Y_k\}_{k=1,\ldots,N_{\rm nuc}})$ and $\omega = \omega(\rho, T, Y_e, Y_\mu, \{Y_k\}_{k=1,\ldots,N_{\rm nuc}})$ for pressure P and specific energy density ω (T is the medium temperature, $N_{\rm nuc}$ the number of nuclear species). Analogously to e^-

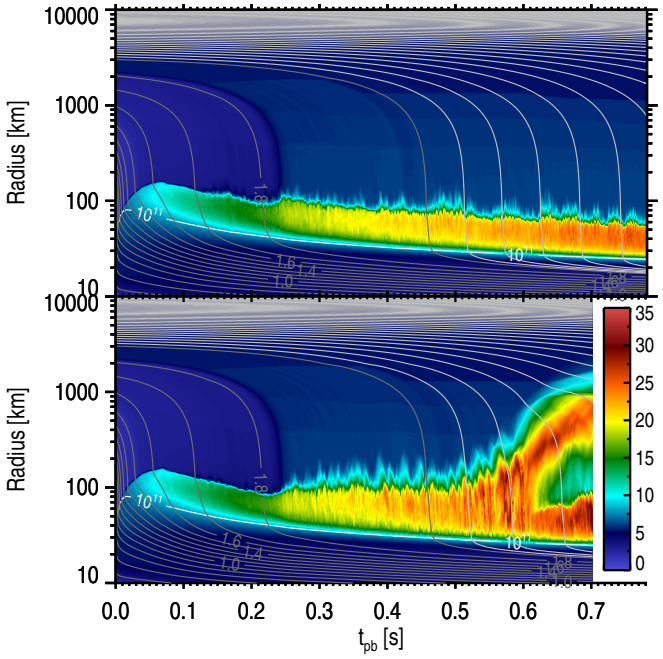


FIG. 2. Evolution of angle-averaged specific entropy (color; in $k_{\rm B}$ per nucleon) vs. post-bounce time for model s20.0-SFHo with our standard physics (*top*) and with muons (*bottom*). The outer boundary of the light blue-green-yellow region follows the average radius of the SN shock. The gray lines mark "mass shells" (radii of constant enclosed baryonic mass), the white line corresponds to an average density of $10^{11}\,{\rm g\,cm^{-3}}$.

and e^+, μ^- and μ^+ provide an additive contribution to P and ω and are treated as ideal Fermi gases of arbitrary degeneracy and arbitrary degree of relativity. In nuclear statistical equilibrium (NSE) the mass fractions of nuclei and nucleons, Y_k, are determined by the Saha equations and hence $Y_k = Y_k(\rho, T, Y_e, Y_\mu)$ holds; otherwise they follow from evolution equations similar to Eq. (4) with Q_ℓ being replaced by source terms for nuclear reaction rates. With ρ, ω, Y_e and Y_μ given as solutions of the hydrodynamics and Y_k ($k = 1, ..., N_{\rm nuc}$) being determined either by NSE or Eq. (4), T and the chemical potentials μ_e, μ_μ, μ_n, μ_p, and μ_k for all k can be determined under the constraint of charge neutrality, $\sum_k Z_k Y_k = Y_e + Y_\mu$, with Z_k being the nuclear charge number of species k.

Accounting for the presence of muons and the differences of the ν and $\bar\nu$ scattering cross sections with nucleons due to nucleon-recoil and weak-magnetism [13], we generalized the neutrino-transport module VERTEX to an energy-dependent six-species treatment, tracking ν_e, $\bar\nu_e$, ν_μ, $\bar\nu_\mu$, ν_τ, and $\bar\nu_\tau$ individually. Besides our "standard" set of neutrino reaction rates listed in Table 1 of [19], we also implemented all relevant neutrino interactions with μ^- and μ^+ as listed in Table I. The detailed kinematics (energy and momentum exchange between reaction partners) were fully taken into account, describing charged leptons as arbitrarily relativistic and arbitrarily degenerate fermions and nucleons as non-relativistic fermions. Neutral and charged-current interactions between neutrinos and nucleons were handled by the formalism of [20, 21], which includes the effects of nucleon correlations by a random-phase approximation (RPA). We generalized the treatment to also include corrections due to neutron and proton mean-field potentials in the β-processes [22–24] and due to the large rest masses of μ^- and μ^+. Weak-magnetism corrections according to [13] are used in all neutral and charged-current neutrino-nucleon interactions (cf. [16]) except in charged-current reactions of ν_μ and $\bar\nu_\mu$ with nucleons (because lepton-mass dependence was neglected in [13]). Neutral and charged-current reactions of neutrinos with nucleons bound in light nuclei (^{2}H, ^{3}H, ^{3}He) were approximated by using the neutrino-nucleon interactions of [25], which slightly overestimates (mainly at low energies) the collective opacity of these reactions compared to the detailed description in [26]. When specified, we included in neutrino-nucleon scatterings virial corrections for the axial response of nuclear matter at low densities [27, 28] and/or applied a strangeness-dependent contribution to the axial-vector coupling coefficient [13] with a value of $g_{\rm A}^{\rm s} = -0.1$, consistent with experimental constraints [29]. The virial corrections were implemented via an effective interaction in the RPA that was stronger at low densities. This yielded results similar to those in [27].

Our SN simulations were performed in 2D for a non-rotating $20\,M_\odot$ progenitor model [30] with the Lattimer-Swesty EoS (LS220) with nuclear incompressibility $K = 220\,{\rm MeV}$ [31] and the SFHo EoS [32, 33] (models s20.0-LS220 and s20.0-SFHo, respectively). After bounce, at densities below $10^{11}\,{\rm g\,cm^{-3}}$, we employed a 23-species NSE solver at $T > 0.5\,{\rm MeV}$ for infalling and $T > 0.34\,{\rm MeV}$ for expanding, high-entropy matter, and nuclear "flashing" [15] at lower temperatures. For the polar coordinate grid we used a time-dependent number of 400–650 radial zones and 160 lateral zones with a refinement to 320 lateral zones outside of the gain radius (i.e., the radius exterior to which neutrino heating dominates), and for the neutrino transport 15 geometrically distributed energy bins with $\epsilon_{\rm max} = 380\,{\rm MeV}$.

Results.—In addition to conducting simulations for the two employed nuclear EoSs with our standard set of neutrino processes (Table 1 in [19]), we also investigated cases where we included (a) the virial corrections in ν-N-scattering, (b) all muon effects, (c) both muon and virial effects, and (d) muons, virial effects, and a strangeness correction in ν-N-scattering. Figure 1 displays the time evolution of the average shock radii for the models with SFHo (top left) and LS220 EoS (top right). It is obvious that muon formation enables an explosion for the SFHo model, which does not explode with standard neutrino physics, and it allows for an earlier onset of the explosion with the LS220 EoS.

Figure 2 compares the evolution of angle-averaged ra-

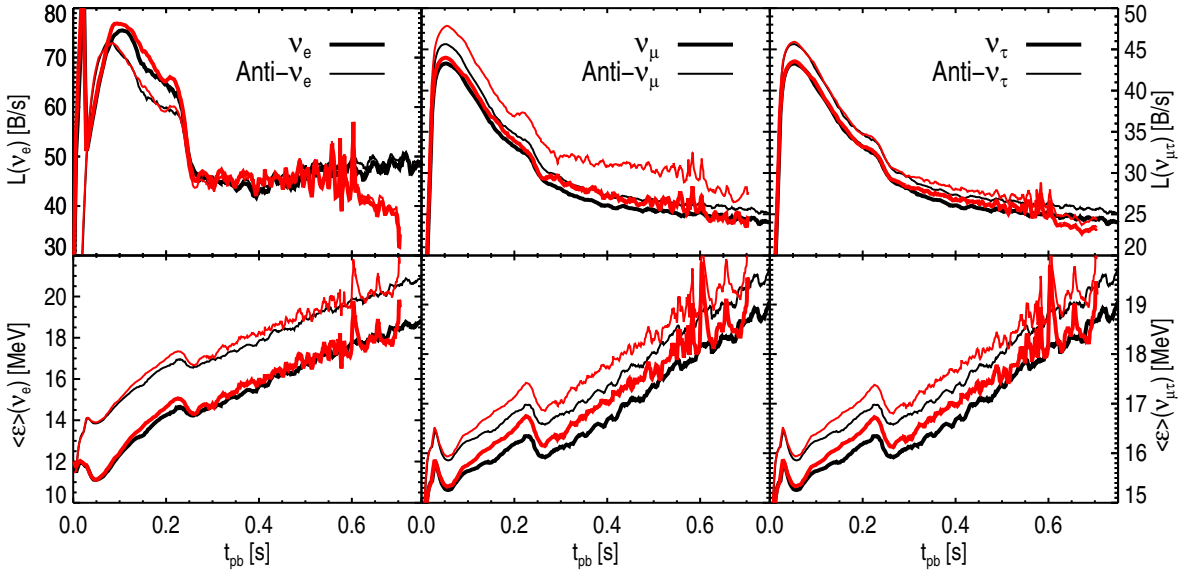


FIG. 3. Neutrino luminosities (*upper row*) and radiated mean neutrino energies (defined as ratio of neutrino energy density to number density; *lower row*) vs. post-bounce time, evaluated in the laboratory frame at the average gain radius for the standard model with SFHo EoS (black) and the simulation with muons (red).

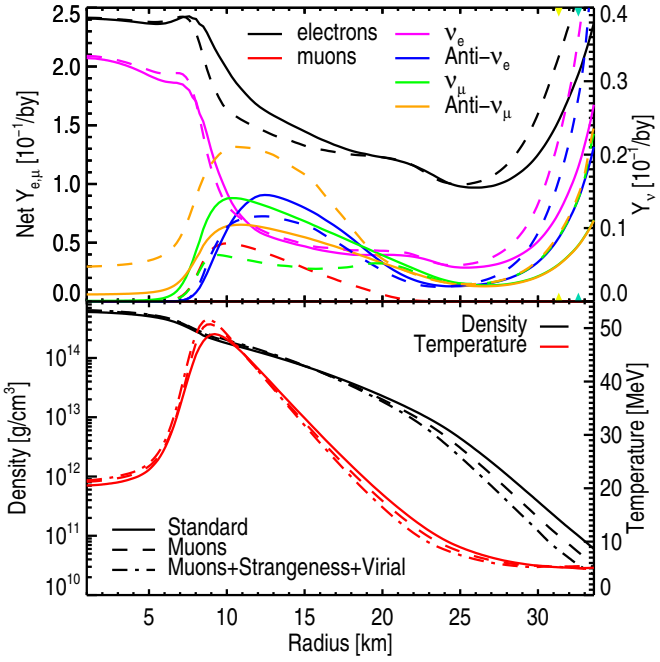


FIG. 4. *Top:* Radial profiles at 0.4 s after bounce of the net numbers of charged leptons (left-hand scale) and neutrinos (right-hand scale) per baryon for the standard model with SFHo EoS (solid) and the simulation with muons (dashed). *Bottom:* Radial profiles of density (black) and temperature (red) for three cases with SFHo EoS.

dial profiles of the entropy per baryon (superimposed in color on mass-shell trajectories) for two SFHo-models. After the arrival of the interface between silicon-shell and oxygen-rich Si-layer at the shock at ∼240 ms p.b., the shock radius in the model with muons is considerably larger than in the standard case, leading to an explosion, despite the inverse order of the shock radii at earlier times (Fig. 1). The lower panels of Fig. 1 provide an explanation: with muons the proto-NS contracts notably faster (left). The creation of μ^- and μ^+ effectively softens the EoS by conversion of thermal and degeneracy energy of e^- into rest-mass energy of muons. In addition, it significantly raises the emission of $\bar{\nu}_\mu$ and, to a lesser extent, also of ν_μ (Fig. 3, middle panels). The accelerated shrinking of the NS leads to higher temperatures at given densities and correspondingly increased luminosities and mean energies of the emitted electron- and tau-flavor neutrinos, which are shown in Fig. 3 (left and right panels) at the gain radius, where ν_e and $\bar{\nu}_e$ differences are relevant for the neutrino heating. As a consequence, the neutrino-heating rate, per baryon as well as integrated over the gain layer (i.e. the region between gain radius and shock), becomes sizeably greater in the model with muons at $t \gtrsim 240$ ms (Fig. 1, bottom right). Muons therefore have a similar overall effect as the strangeness-dependent reduction of neutrino-nucleon scattering discussed in [3].

Figure 4 documents the appearance of significant charged-muon number (up to $Y_\mu \sim 0.05$) (at the expense of e^-) correlated with a temperature maximum in the NS between ∼7 km ($\sim 4 \times 10^{14}$ g cm^{-3}) and ∼21 km ($\sim 2 \times 10^{13}$ g cm^{-3}). While in the model without muons ν_μ are more abundant than $\bar{\nu}_\mu$, equivalent to the situation for ν_τ and $\bar{\nu}_\tau$ discussed above, the situation is reversed when muons are included: Y_{ν_μ} drops in its peak to about half of the abundance in the standard case, whereas the

number of $\bar{\nu}_\mu$ more than doubles ($Y^{\max}_{\bar{\nu}_\mu} \gtrsim 0.02$).

Including also strangeness corrections in ν-N scattering leads to even faster explosions (Fig. 1, upper panels), because muon and strangeness effects drive the system in the same direction, namely a faster contraction of the NS (Fig. 1, bottom left). The situation for virial effects is ambiguous. While the LS220 model with virial corrections explodes faster than the standard case and evolves similar to the simulation with muons, virial effects in addition to muons make little difference (Fig. 1, top right). In contrast, an SFHo model including virial corrections and strangeness $g^{\rm s}_{\rm A} = -0.1$ (not shown) explodes only later than 600 ms due to the strangeness effects, whereas the SFHo models with virial response fail to explode with and without muons (Fig. 1, top left). For relevant temperatures ($T \approx 5$–$10\,$MeV) virial effects lead to a reduction of the ν-N-scattering opacity compared to RPA results only at densities below $\sim(0.01 \ldots 0.03)\rho_0$. This is so low that there is a visible (1–2%) increase of the heavy-lepton neutino emission but hardly any correspondingly accelerated contraction of the NS radius (Fig. 1, bottom left). Virial effects are therefore subtle, because they can enhance energy extraction in the ν_μ and ν_τ sector without explosion-favoring consequences for emission and heating by ν_e and $\bar{\nu}_e$.

Conclusions.—We have demonstrated by 2D simulations that the appearance of muons in the hot medium causes enhanced neutrino emission and faster contraction of the proto-NS with supportive effects on the neutrino-energy deposition behind the stalled shock and the onset of neutrino-driven explosions. The ongoing muonization of the new-born NS may also lead to stronger heating of matter that is still accreted and re-ejected after the onset of the explosion (see [8] and references therein) and could therefore raise the explosion energy. Muonization mainly affects more massive and thus hotter NSs and should have less impact on SN explosions with less massive NSs. Final conclusions about their detailed role in the explosion will require 3D simulations. Since muon formation effectively softens the NS EoS at high densities, it also has important implications for the collapse of hot NSs to BHs [34]. Therefore muons cannot be ignored in detailed models of the SN explosion mechanism and NS formation. For a rigorously self-consistent description, this requires —and we have implemented— a full six-species treatment of neutrino transport, which couples the production of electron- and muon-flavor neutrinos. Since all six neutrino species differ in their spectra, corresponding transport results may offer interesting new aspects for neutrino oscillations. Muons may also have to be included in simulations of NS-NS mergers, because the compactness of the merger remnant and its time scale for a possible collapse to a BH is sensitive to muon formation in the hot nuclear medium.

We acknowledge hospitality by ECT* in Trento during the MICRA 2013 workshop, where discussions helped start this work. At Garching, this work was supported by the European Research Council through grant ERC AdG 341157-COCO2CASA and by the Deutsche Forschungsgemeinschaft through grants SFB 1258 ("Neutrinos, Dark Matter, Messengers") and EXC 153 ("Excellence Cluster Universe"). GMP acknowledges partial support by the Deutsche Forschungsgemeinschaft through grant SFB 1245 ("Nuclei: From Fundamental Interactions to Structure and Stars"). CJH was supported in part by US DOE Grants DE-FG02-87ER40365 and DE-SC0008808. The numerical simulations were carried out at the Max Planck Computing and Data Facility (MPCDF).

[1] T. Takiwaki, K. Kotake, and Y. Suwa, Astrophys. J. **786**, 83 (2014), arXiv:1308.5755.
[2] T. Melson, H.-T. Janka, and A. Marek, Astrophys. J. Lett. **801**, L24 (2015), arXiv:1501.01961.
[3] T. Melson *et al.*, Astrophys. J. Lett. **808**, L42 (2015), arXiv:1504.07631.
[4] E. J. Lentz *et al.*, Astrophys. J. Lett. **807**, L31 (2015), arXiv:1505.05110.
[5] H.-T. Janka, T. Melson, and A. Summa, Ann. Rev. Nucl. Part. Sci. **66**, 341 (2016), arXiv:1602.05576.
[6] L. F. Roberts *et al.*, Astrophys. J. **831**, 98 (2016), arXiv:1604.07848.
[7] B. Müller, Publ. Astron. Soc. Australia **33**, e048 (2016), arXiv:1608.03274.
[8] B. Müller, T. Melson, A. Heger, and H.-T. Janka, Monthly Not. Royal Astron. Soc. **472**, 491 (2017), arXiv:1705.00620.
[9] A. W. Steiner, M. Prakash, J. M. Lattimer, and P. J. Ellis, Phys. Reports **411**, 325 (2005), nucl-th/0410066.
[10] M. G. Alford and G. Good, Phys. Rev. C **82**, 055805 (2010), arXiv:1003.1093.
[11] A. Lohs, G. Martínez-Pinedo, and T. Fischer, Charged Current Interactions of numu Neutrinos in Supernova, in *XIII Nuclei in the Cosmos (NIC XIII)*, p. 118, 2014.
[12] A. Marek, H.-T. Janka, R. Buras, M. Liebendörfer, and M. Rampp, Astron. Astrophys. **443**, 201 (2005), astro-ph/0504291.
[13] C. J. Horowitz, Phys. Rev. D **65**, 043001 (2002), astro-ph/0109209.
[14] C. J. Horowitz and G. Li, Phys. Lett. B **443**, 58 (1998), hep-ph/9809492.
[15] M. Rampp and H.-T. Janka, Astron. Astrophys. **396**, 361 (2002), astro-ph/0203101.
[16] R. Buras, M. Rampp, H.-T. Janka, and K. Kifonidis, Astron. Astrophys. **447**, 1049 (2006), astro-ph/0507135.
[17] A. Marek, H. Dimmelmeier, H.-T. Janka, E. Müller, and R. Buras, Astron. Astrophys. **445**, 273 (2006), astro-ph/0502161.
[18] B. Fryxell, E. Müller, and D. Arnett, Hydrodynamics and nuclear burning, in *preprint MPA-449*, 1989.
[19] H.-T. Janka, Ann. Rev. Nucl. Part. Sci. **62**, 407 (2012), arXiv:1206.2503.
[20] A. Burrows and R. F. Sawyer, Phys. Rev. C **58**, 554 (1998), astro-ph/9801082.
[21] A. Burrows and R. F. Sawyer, Phys. Rev. C **59**, 510

(1999), astro-ph/9804264.
[22] S. Reddy, M. Prakash, and J. M. Lattimer, Phys. Rev. D **58**, 013009 (1998), astro-ph/9710115.
[23] G. Martínez-Pinedo, T. Fischer, A. Lohs, and L. Huther, Phys. Rev. Lett. **109**, 251104 (2012), arXiv:1205.2793.
[24] L. F. Roberts, S. Reddy, and G. Shen, Phys. Rev. C **86**, 065803 (2012), arXiv:1205.4066.
[25] S. W. Bruenn, Astrophys. J. Suppl. **58**, 771 (1985).
[26] T. Fischer *et al.*, Expected impact from weak reactions with light nuclei in corecollapse supernova simulations, in *European Physical Journal Web of Conferences*, , European Physical Journal Web of Conferences Vol. 109, p. 06002, 2016, arXiv:1512.00193.
[27] C. J. Horowitz, O. L. Caballero, Z. Lin, E. O'Connor, and A. Schwenk, Phys. Rev. C **95**, 025801 (2017), arXiv:1611.05140.
[28] Z. Lin and C. J. Horowitz, ArXiv e-prints (2017), arXiv:1708.01788.
[29] T. J. Hobbs, M. Alberg, and G. A. Miller, Phys. Rev. C**93**, 052801 (2016), arXiv:1601.01729.
[30] S. E. Woosley and A. Heger, Phys. Reports **442**, 269 (2007), astro-ph/0702176.
[31] J. M. Lattimer and F. Douglas Swesty, Nuclear Physics A **535**, 331 (1991).
[32] M. Hempel, T. Fischer, J. Schaffner-Bielich, and M. Liebendörfer, Astrophys. J.**748**, 70 (2012), arXiv:1108.0848.
[33] A. W. Steiner, M. Hempel, and T. Fischer, Astrophys. J. **774**, 17 (2013), arXiv:1207.2184.
[34] A. Summa, R. Bollig, H.-T. Janka, and T. Melson, in preparation (2017).